CrossMark

The Role of Work Function and Band Gap in Resistive Switching Behaviour of ZnTe Thin Films

SRINU ROWTU,[1] L.D. VARMA SANGANI,[1]
and M. GHANASHYAM KRISHNA (iD)[1,2]

1.—Centre for Advanced Studies in Electronics Science and Technology, School of Physics, University of Hyderabad, Hyderabad, Telangana 500046, India. 2.—e-mail: mgksp@uohyd.ernet.in

Resistive switching behavior by engineering the electrode work function and band gap of ZnTe thin films is demonstrated. The device structures Au/ZnTe/Au, Au/ZnTe/Ag, Al/ZnTe/Ag and Pt/ZnTe/Ag were fabricated. ZnTe was deposited by thermal evaporation and the stoichiometry and band gap were controlled by varying the source–substrate distance. Band gap could be varied between 1.0 eV to approximately 4.0 eV with the larger band gap being attributed to the partial oxidation of ZnTe. The transport characteristics reveal that the low-resistance state is ohmic in nature which makes a transition to Poole–Frenkel defect-mediated conductivity in the high-resistance states. The highest R_{off}-to-R_{on} ratio achieved is 10^9. Interestingly, depending on stoichiometry, both unipolar and bipolar switching can be realized.

Key words: ZnTe, thin films, resistive switching, work function, band gap

INTRODUCTION

The majority of materials employed in resistive switching or resistive random access memory (RRAM) devices are oxides. In general, the processing of oxide thin films requires high substrate temperature which leads to additional complexity in the fabrication of devices. Another issue is the relatively high dielectric constant of most oxides resulting in high breakdown voltages. A frequently reported and common strategy to decrease forming voltage is to change the electrode materials. An alternative approach to resolving this issue is to employ lower-dielectric-constant non-oxide materials as active layers in RRAM devices.[1–10]

One class of materials that may be of interest in this context, but have not been investigated thoroughly are the II–VI compound semiconductors, although they have been the focus of interest for application in optical, optoelectronic electronic and photovoltaic applications.[11]

ZnTe is a II–VI semiconductor that intrinsically shows p-type conduction. The band gap energy can be tuned by varying the Zn-to-Te ratio and values between 1 eV and 2.3 eV have been reported.[12–15] It is also known that the low-frequency dielectric constant of ZnTe is 9.8.[16] Notwithstanding these interesting properties, research on application of ZnTe as an active layer in resistive switching devices is limited. The first report was by Ota and Takahashi[17] followed by the work of Burgelman.[18] More recently, Ananthan et al.[19] reported a ZnTe-based RRAM device in which the ZnTe layer was prepared using atomic layer deposition.

In view of the promise shown, there is need for further investigations on ZnTe-based RRAM devices. The deposition of ZnTe thin films by thermal evaporation and resulting optical properties have been reported earlier by our group.[13–15] In this paper, we examine the potential of thermally evaporated ZnTe thin films for RRAM applications. Metal electrode-driven variation in resistive switching behavior, induced by work-function differences, is also reported.

EXPERIMENTAL

ZnTe thin films were deposited by thermal evaporation from a ZnTe source in a high vacuum of 8×10^{-6} mbar. The substrates, glass and Si (100)

were not heated during deposition. The substrate to source distance was varied between 5 cm and 18 cm to investigate its effect on structure microstructure, chemical composition and optical properties. The crystalline nature in the films was determined by recording x-ray diffraction (XRD) patterns in a powder diffractometer (Bruker Discovery D8) with Cu Kα radiation of wavelength = 0.15406 nm. The surface morphology was examined in a field emission scanning electron microscope (FE-SEM, Carl Zeiss model Ultra 55). The spectral transmission curves were recorded in a double-beam spectrophotometer scanning in the wavelength range of 200–2500 nm (JASCO model V-670). Surface roughness of the films was measured in a surface profiler (XP-100, Ambios Technology, USA).

The fabrication of RRAM cells comprised the following steps: (1) The bottom electrode layers are Au, Pt or Al. In the case of Au, a Cr layer is first deposited by electron beam evaporation (as a glue layer) followed by Au deposition using thermal evaporation. Al is directly deposited using thermal evaporation, whereas for Pt, a pre-coated Si wafer is used. Typical bottom electrode size is 10–80 μm with a thickness of 100 nm and is patterned by using photo-lithography followed by lift-off and ZnTe layer deposition by thermal evaporation. Finally, the top electrode is patterned on the ZnTe layer using photolithography followed by the lift-off process. Al and Au are deposited as top electrodes. In some cases, Ag dots are also employed. The photograph of a typical fabricated device where the top and bottom electrodes are gold with a 20 μm $\times$ 20-μm size is shown in Fig. 1. The fabricated cell is characterized using an Agilent B1500 semiconductor device analyzer, and switching behavior is observed by using direct current (DC) voltage sweep measurements with the bottom electrode being grounded. Although films with different thicknesses were deposited, it was found that 50 nm was too low, resulting in shorting of the top and bottom electrodes. Additionally, films with thickness greater than 150 nm did not show switching behavior. Hence, only films of thickness between 100 nm and 150 nm could be tested and a thickness-dependent study could not be performed.

RESULTS AND DISCUSSION

RRAM devices require films with thicknesses of the order of few tens of nm which is difficult to achieve reproducibly in thermal evaporation. Hence, it is necessary to carry out optimization experiments to achieve the desired thickness of ZnTe films. This was done by evaporating fixed quantities of source material at a constant power, fixed source–substrate distance and varying the duration. Two weights of source material, 0.1 g and 0.3 g, were considered and the variation in thickness as a function of deposition time was investigated at source–substrate distances of 5 cm, 10 cm,
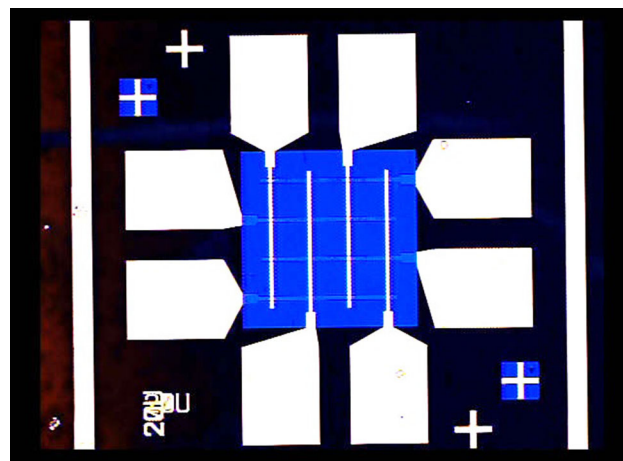

Fig. 1. Photograph of a RRAM device with 20 μm $\times$ 20-μm electrodes.
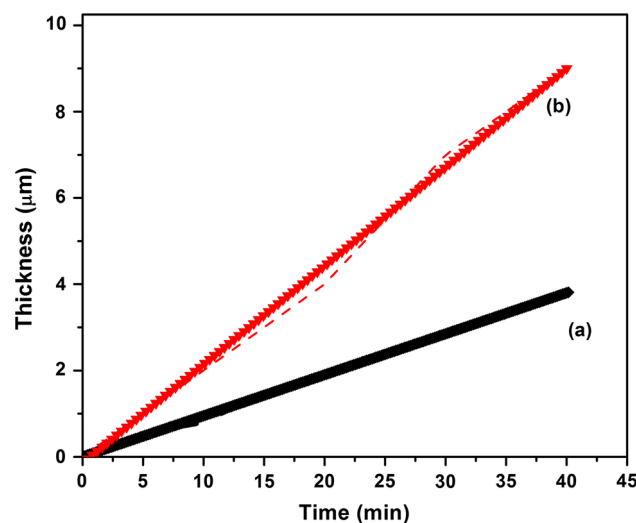

Fig. 2. Variation in thickness as a function of duration of deposition at a source–substrate distance of 5 cm and two different precursor weights (a) 0.1 g and (b) 0.3 g.

and 18 cm. The results of a typical experiment carried out at a substrate–source distance of 5 cm are shown in Fig. 2a and b. It is evident that the variation is linear and thicknesses as high as 9 μm can be obtained within 40 min for 0.3 g of source material. In contrast, the highest thickness achieved was approximately 1.5 μm for 0.1 g of source material. The rates of deposition were 0.1 μm/min and 0.25 μm/min, respectively, for 0.1 g and 0.3 g of source material.

FE-SEM images of the 50-nm-, 100-nm-, and 200-nm-thick films deposited at source–substrate distances of 10 cm and 18 cm are shown in Figs. 3a, b, and c and 4a, b, and c, respectively. The films deposited at 10 cm show spherical grains that are densely packed with no evidence for voids or pores. The average grain size is 12 nm, 24 nm, and 46 nm for the films with thicknesses of 50 nm, 100 nm, and
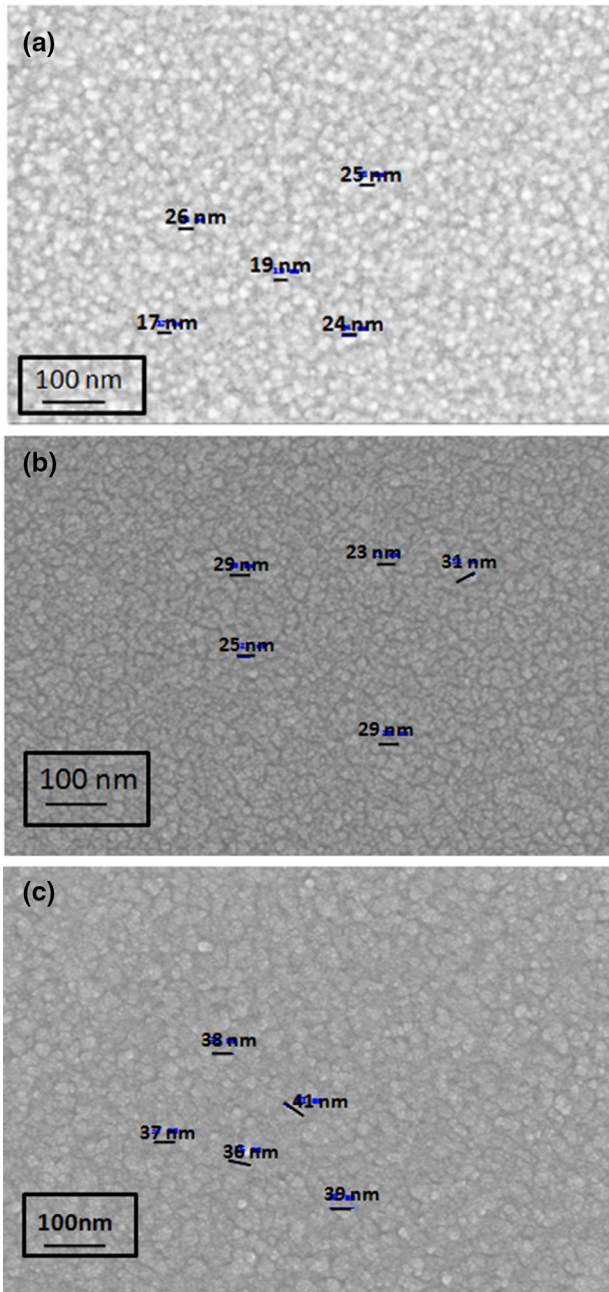
Fig. 3. FE-SEM images of the films deposited at a source–substrate distance of 18 cm and nominal thickness of (a) 50 nm, (b) 100 nm, and (c) 200 nm.

Fig. 4. FESEM images of the films deposited at a source–substrate distance of 10 cm and nominal thickness of (a) 50 nm, (b) 100 nm, and (c) 200 nm.

200 nm, respectively. When the distance is increased to 18 cm, the morphology still consists of spherical grains and average grain sizes are 22 nm, 27 nm, and 32 nm for the 50-nm-, 100-nm-, and 200-nm-thick films, respectively. There is evidence of cracks in the films which were absent in the case of films deposited at a distance of 10 cm. Thus, there is an overall decrease in the grain size with increase in source–substrate distance. This decrease in grain size can be attributed to the decrease in rate of deposition which is further confirmed by the
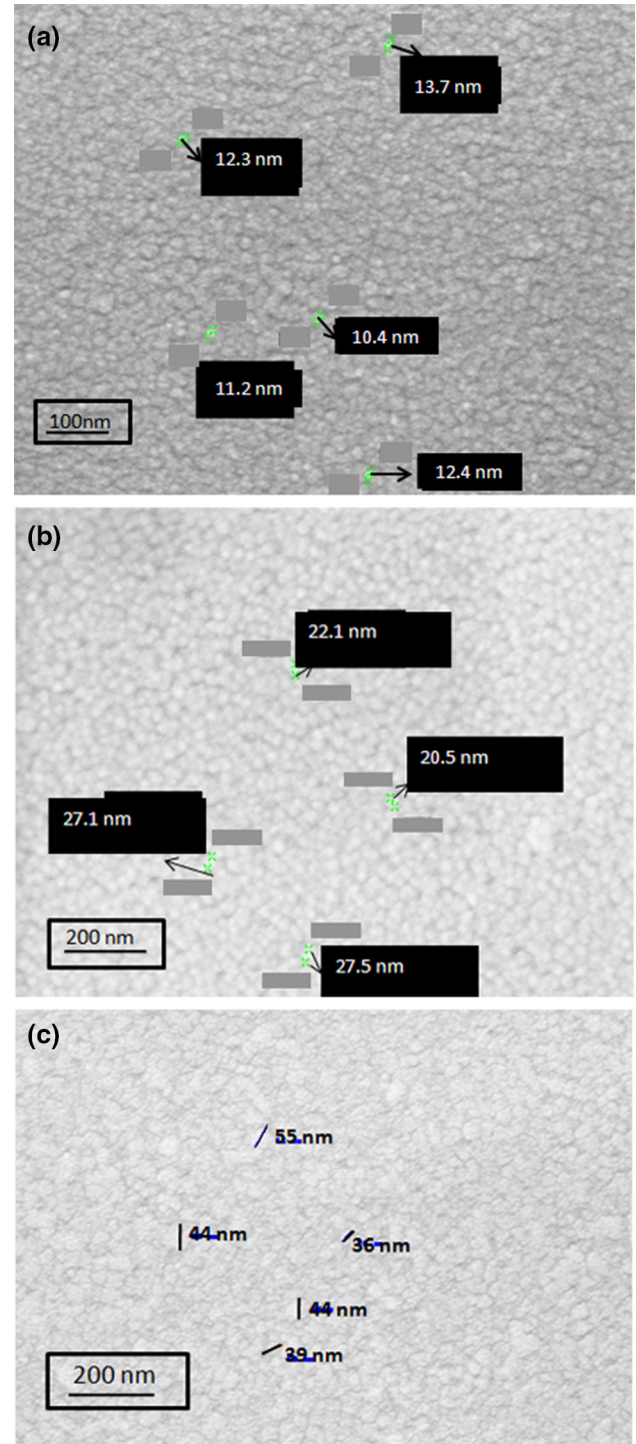
morphology of the films deposited at a source–substrate distance of 5 cm. At this distance, the rate of deposition is much higher and less controllable. Hence, films of 850-nm and 1000-nm thickness were examined for morphology as shown Fig. 5a and b. The grain size of film with thickness 1000 nm is

236 nm and the grains are arranged in a periodic form. The grain size of 850-nm-thick films is 141 nm. The grains in this case are decorated by smaller 30-nm nanoparticles. The average surface roughness of all the films measured using a diamond stylus-based profiler is 2–8 nm.

The chemical composition of these films was investigated using EDX spectroscopy. The results for different source–substrate distances are given in Table I. A point to note is that the melting point of Zn at 419.53°C is low compared with tellurium at 449.51°C. The weight percents of Zn and Te for stoichiometric ZnTe should be 34% and 66%, respectively. Since the Zn melting point is lower,

incongruent evaporation leading to the films being Zn-rich is expected. An important question that arises is whether the Zn-to-Te ratio is source–
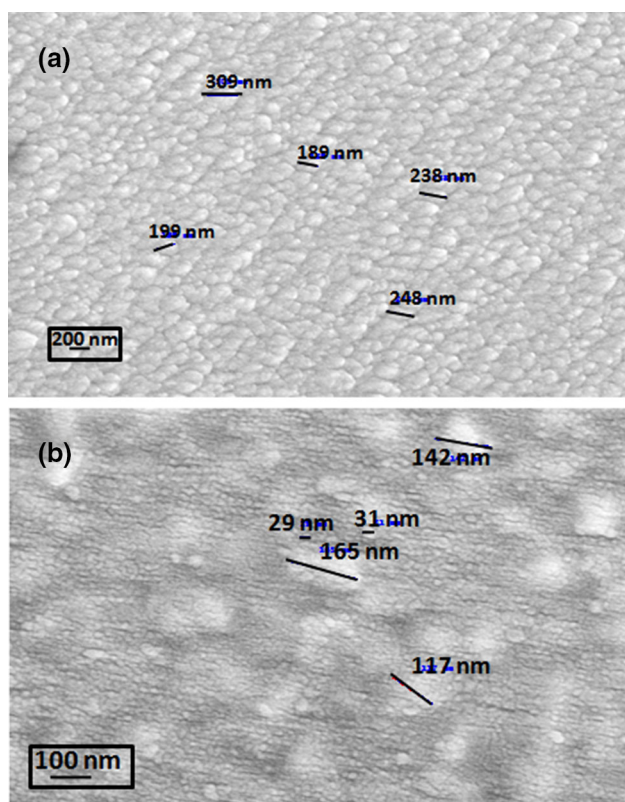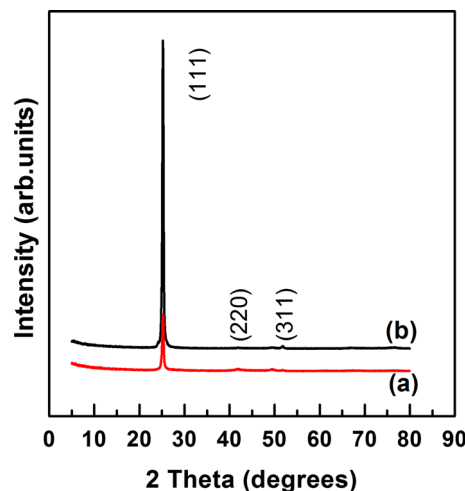

Fig. 6. X-ray diffraction pattern of ZnTe films deposited on BSG substrates at a source–substrate distance of 5 cm and thickness of (a) 850 nm and (b) 1000 nm.
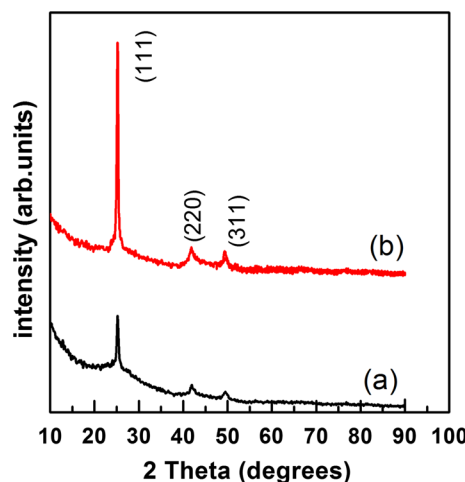

Fig. 7. X-ray diffraction pattern of ZnTe films deposited on BSG substrates at a source–substrate distance of 10 cm and thickness of (a) 100 nm and (b) 200 nm.

Fig. 5. FE-SEM images of the films deposited at a source–substrate distance of 5 cm and nominal thickness of (a) 1000 nm and (b) 850 nm.

Table I. EDX data for films deposited at different source–substrate distances on glass substrates

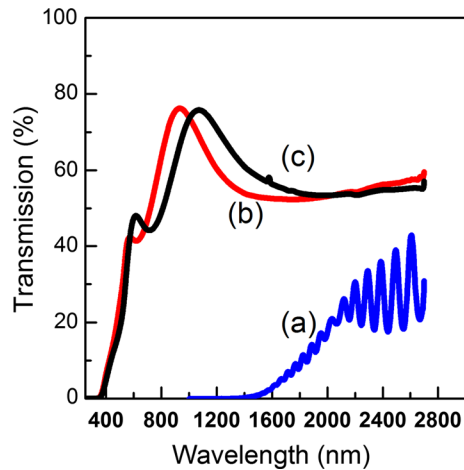| | Source–substrate distance (films are deposited on BSG) | | | | | |
| | 18 cm | | 10 cm | | 5 cm | |
Element	at.%	wt.%	at.%	wt.%	at.%	wt.%
Zn	15.48	27.09	19.03	25.20	50.20	34.07
Te	9.01	30.76	19.32	49.93	49.73	65.89
O	45.18	19.35	41.69	13.51	–	–
Si	30.33	22.80	19.96	11.36	–	–

Fig. 8. Measured spectral transmission curves for the ZnTe films deposited at a source–substrate distance of (a) 5 cm (approximate thickness 5000 nm), (b) 10 cm and (c) 18 cm (the approximate thickness in (b) and (c) is 200 nm).

substrate distance-dependent and, therefore, rate of deposition-dependent or not. Clearly, at large distances (18 cm) the films are Zn-rich, while at shorter distances (5 cm and 10 cm), the films are more stoichiometric. The reason for this is that the process of heating during evaporation leads to dissociation of the source materials. As a consequence, the lower-melting-point component (Zn in the present case) evaporates first, leading to a film composition that is rich in this element. At lower distances, since the rates of deposition are higher, the deviation from stoichiometry is not so pronounced.

The XRD patterns of ZnTe films deposited on glass substrates at a source–substrate distance of 5 cm are shown in Fig. 6a and b for thicknesses of 1000 and 850 nm. The films show a very strong preferred (111) orientation with low-intensity peaks corresponding to the (220) and (311) planes. When the source–substrate distance is increased to 10 cm, the films are more nanocrystalline, as evidenced from the presence of an amorphous background. It is observed in the XRD patterns in Fig. 7a and b, of the 100-nm- and 200-nm-thick films, that there are three peaks at $2\theta = 25.276°$, $41.92°$, and $49.6°$, corresponding to the (111), (220) and (311) planes of the face-centered cubic structure of ZnTe, respectively (PCPDF WIN file number 893054). It is to be noted that these are typical XRD patterns corresponding to the thickness of films for which SEM images are presented in Figs. 4 and 5. From the XRD patterns, it is evident that the films crystallize even though the substrates are not subjected to any heat treatment during deposition.

The spectral transmission of the ZnTe films with different thicknesses at a source–substrate distance of 5 cm, 10 cm, and 18 cm is shown in Fig. 8a, b, and c, respectively. The transmission curves display interference fringes due to the multiple reflections

at the film-air, film-substrate and substrate-air interfaces that occur due to the refractive index contrast between the three media. The fringe pattern can be used to estimate the refractive index, absorption coefficient and band gap as described in detail elsewhere.[8–10] The relevant parameter for this work is the band gap and it is observed that the band gap decreases with thickness. The expected bandgap value for stoichiometric ZnTe is between 1 eV and 2 eV. However, for the films deposited at source–substrate distances of 10 cm and 18 cm, the band gap is much larger. The large band gap could be due to partial oxidation of Zn to ZnO which is known to have a bandgap between 3.3 eV and 4.0 eV. As the source–substrate distance is decreased to 5 cm there is drastic decrease in the transmission and the band gap, as shown in Fig. 8c. The band gaps of the films deposited at 5 cm were in the range of 2.3–1.15 eV. In contrast, the band gaps of the films deposited at 10 cm and 18 cm were 3.8–4.0 eV.

The refractive index of the films is related to the height of the fringes which, for a homogeneous film, should be constant at wavelengths above the band gap. It is observed in the present case that the height of fringes is not constant and is wavelength-dependent, which is an indication of optical inhomogeneity in the films. There are two main sources of the optical inhomogeneity; one is microstructural in origin and the other is related to variation in chemical composition across the thickness of the films.[20] Thin films prepared by thermal evaporation typically display a columnar microstructure. If the dimensions of the columns are not constant, then this leads to variations in refractive index. An issue that is particularly relevant to thermal evaporation is the variation in chemical composition across the thickness of the films. As stated earlier, incongruent evaporation of ZnTe is expected due to the difference in melting points of the two elements. As a result, the initial layers may be Zn-rich while the subsequent layers are more stoichiometric. Therefore, the refractive index varies across the thickness of the films and this is manifested as a variation in height of the fringes in the interference pattern. Thus, from a simple examination of the spectral transmission curves, it can be inferred that there is a chemical composition gradient in the films. The films exhibit non-stoichiometry which is source–substrate distance-dependent and, therefore, rate of deposition-dependent. The optical response is clearly more sensitive to changes in stoichiometry than XRD. This is evident from the fact that XRD patterns indicate that there are portions of the films which are stoichiometric ZnTe but provide no evidence for the non-stoichiometric or oxidized parts of the films.

In resistive switching devices, the work function contrast between the metal electrodes and the dielectric is an extremely crucial performance-determining step. This can be discussed in the context
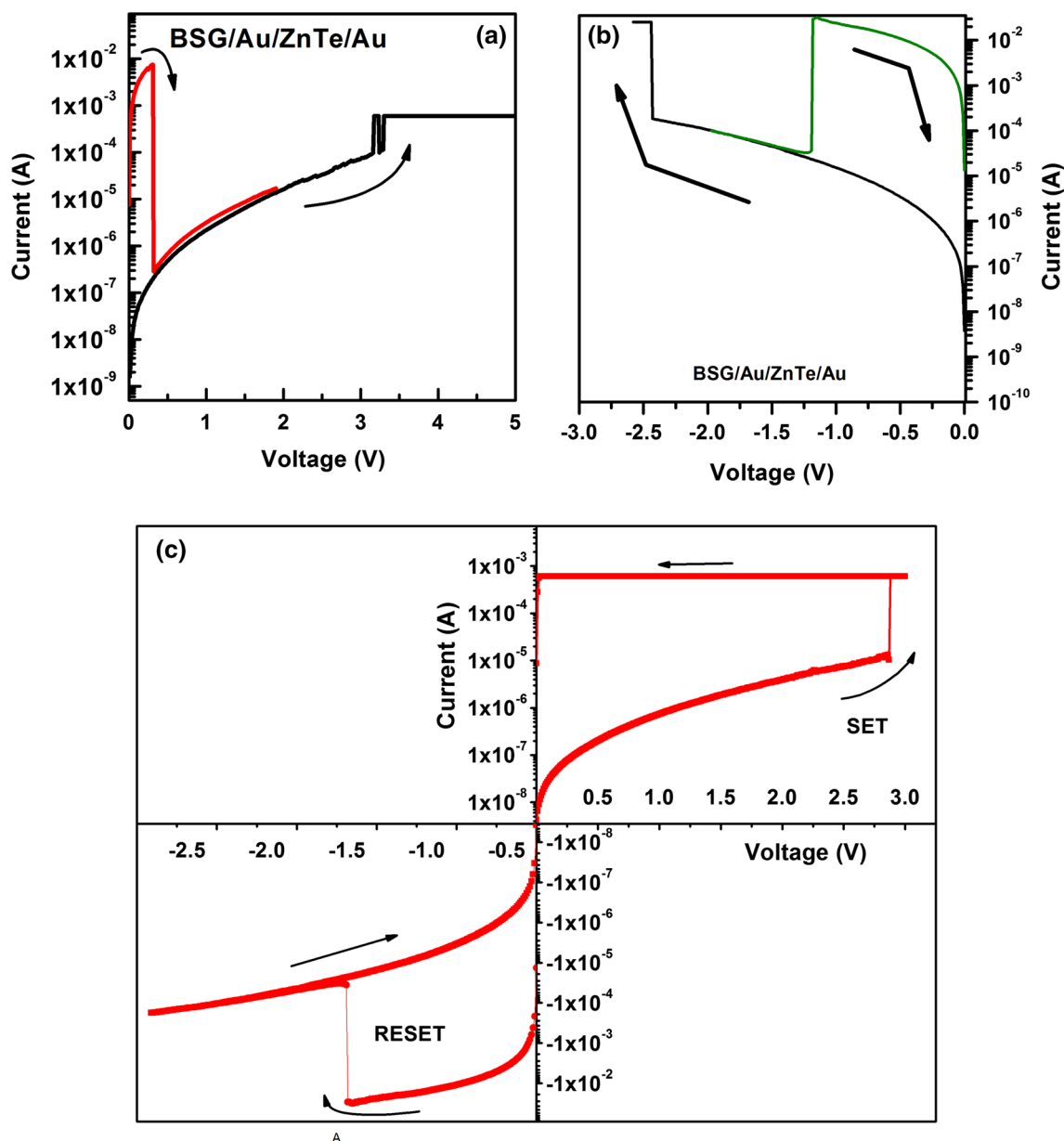
Fig. 9. I–V characteristics of the RRAM device with the structure Au/ZnTe/Au showing (a) unipolar switching in the positive direction, (b) unipolar switching in the negative direction and (c) bipolar switching.

of the barrier heights for metal–semiconductor junctions. It is to be noted that the junction between the bottom electrode and ZnTe is a Schottky barrier. The question that needs to be addressed is whether the choice of bottom electrode has any role to play in determining the switching characteristics. To understand this, several device structures as listed below were fabricated (in the sequence bottom electrode/ZnTe/top electrode).

1. Au/ZnTe/Au; 2. Au/ZnTe/Ag; 3. Al/ZnTe/Ag and 4. Pt/ZnTe/Ag. The relevant parameters to note are that the electron affinity of ZnTe is 3.53 eV.[21] The work functions of Pt, Au, Ag and Al are 5.68 eV, 4.8–5.2 eV, 4.3–4.6 eV, and 3.4–4.4 eV, respectively.[22]

For an ideal metal p-type semiconductor interface, the Schottky barrier height φ_{bp}

$$\varphi_{bp} = E_g/q + c - \Phi_M \qquad (1)$$

where E_g is the band gap, χ is the electron affinity of the semiconductor and Φ_M is the metal work function. Assuming that the metal work function is a constant, the barrier height is then determined by the electron affinity and the band gap of the semiconductor. In the previous sections, it was shown that band gap of the films varies from 1.1 eV to 3.9 eV. The results in the following section demonstrate the importance of band gap and electrode materials.
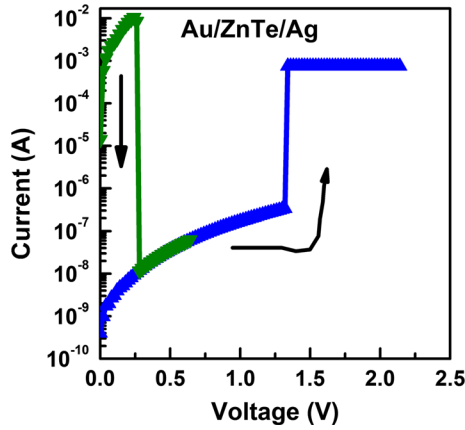
Fig. 10. I–V characteristics of the RRAM device with the structure Au/ZnTe/Ag showing unipolar switching.
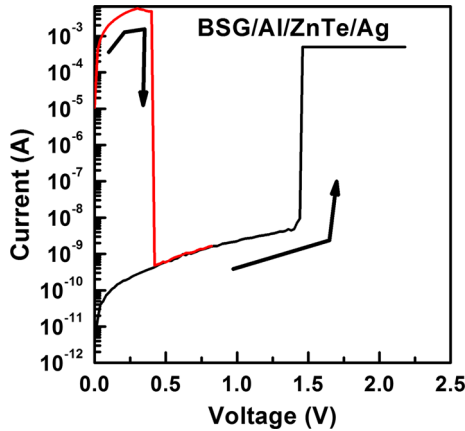

Fig. 11. I–V characteristics of the RRAM device with the structure Al/ZnTe/Ag showing unipolar switching.
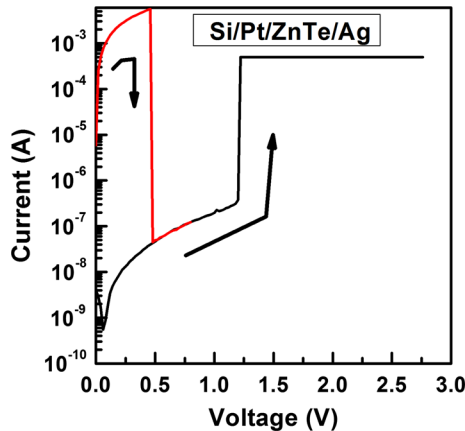

Fig. 12. I–V characteristics of the RRAM device with the structure Pt/ZnTe/Ag showing unipolar switching.
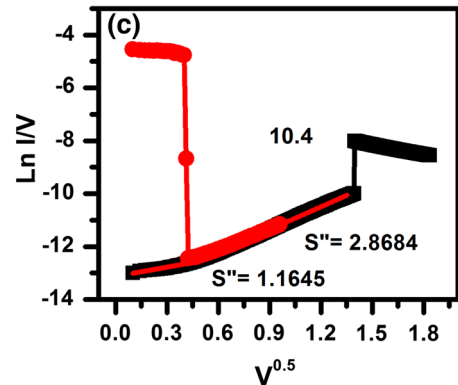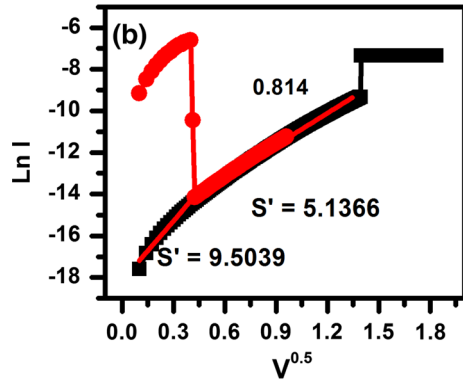

Fig. 13. Double-log plots of the I–V characteristics of the Au/ZnTe/Au structure showing the fits to the (a) ohmic conductivity model, (b) Schottky conduction and (c) Poole–Frenkel type conductivity model.

The first experiment was carried out with the structure Au/ZnTe/Al wherein the ZnTe was deposited at a source–substrate distance of 18 cm. At this distance, the ZnTe has a band gap > 3 eV. The I–V
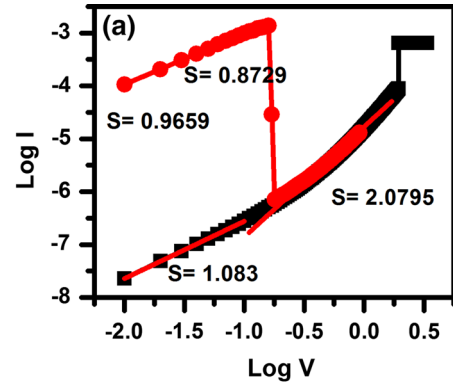
characteristics of this structure indicated that there is no switching even at an applied voltage of 10 V. The structure has high initial resistance in the order of 10^6–10^9 Ω. However, when the top electrode is changed from Al to Au, switching is observed as seen from from Fig. 9a, b, and c. The forming voltage for this device is 3.91 V. Interestingly, the I–V characteristics of the device with the structure Au/ZnTe/Au and 20 μm × 20-μm size exhibit both unipolar and bipolar switching. The initial resistance of the films which was of the order of 10^9 Ω decreases to 10^5 Ω as the bias is increased to 2.8 V, i.e. the fabricated cell is initially in the high-
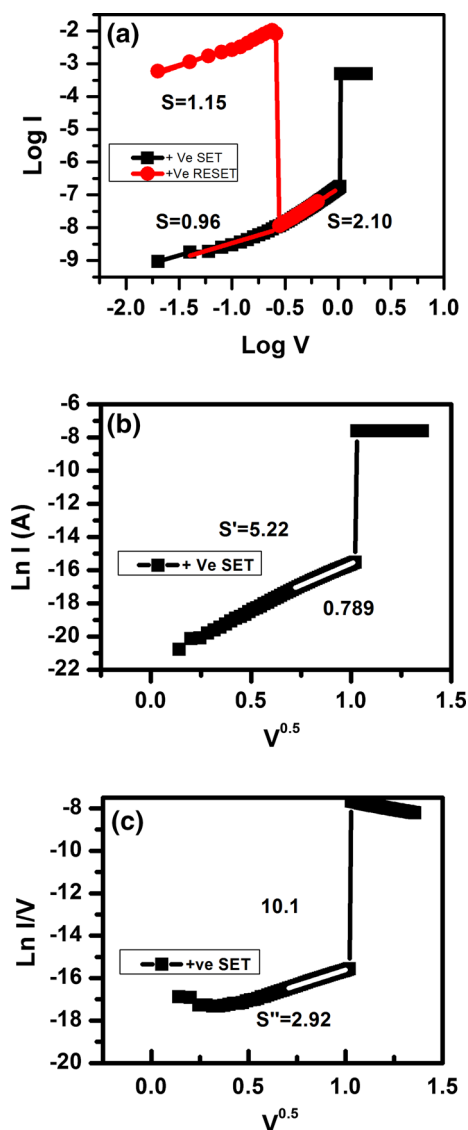
Fig. 14. Double-log plots of the I–V characteristics of the Au/ZnTe/Ag structure showing the fits to the (a) ohmic conductivity model, (b) Schottky conduction model and (c) Poole–Frenkel type conductivity model.

resistance state (HRS). The dielectric breakdown occurs at voltages around 2.8–3.5 V with a compliance current of 0.5 mA. In the set process, due to the breakdown of the ZnTe layer, the resistance of the layer decreases and the cell switches from the HRS to the low-resistance state (LRS). In the reset process, by sweeping the voltage between 0.3 V and 0.61 V, the cell switches from LRS to HRS and the cell draws a current of 7.5–19 mA. It is to be noted that the set voltage and the reset voltages are positive. To check if this process is unipolar or bipolar, polarity of the bias was reversed, and it is indeed seen that the set voltage is positive and reset voltage is negative. The switching of HRS to LRS occurred above 1.94 V and the switching of LRS to HRS is -0.13 V, -0.28 V, and -0.69 V with currents of 1.1 mA, 6 mA, and 16 mA, respectively.

Evidently, the higher work function of gold results in lowering of the barrier height, as expected from Eq. 1, with band gap being constant.

The I–V characteristics of a device with the structure Au/ZnTe/Ag where the ZnTe is deposited at a distance of 10 cm with band gap close to 2 eV and a thickness of 100 nm is shown in Fig. 10. It is also evident in this case that switching behavior is exhibited. There is, however, a slight difference in behavior as compared to the previous structure. In this case, the forming voltage is 2.48 V. It is observed from the I–V characteristics that for both set and reset operations, positive voltages are applied, indicating unipolar switching. The set operation occurs at voltages between 0.44 V and 1.94 V with a compliance current of 0.5 mA. For the reset operation, the cell draws 8–15.6 mA for the voltages of 0.26–0.62 V. In the case when negative voltages were applied for both the set and reset operations, the set operation occurs at voltages between -0.32 V and -0.72 V with a compliance current of 0.5 mA and the reset operation occurs at a current of 3.9–10.6 mA over the voltage range of -0.14 V to -0.26 V.

The impact of changing the bottom electrode from Au to Al and Pt is shown in Figs. 11 and 12, respectively. The forming voltages are 3.76 V and 2.7 V for Al and Pt, respectively. The R_{off}-to-R_{on} ratio is of the order of 10^9 (Fig. 11), when Au is replaced with Al. The first switching occurs at a voltage of 3.76 V, after which the set voltage decreases to 0.78 V. For the reset process, the memory cell drew a current of 1.4–12.6 mA. The memory cell fabricated with a ZnTe layer thickness of 158 nm is in the HRS in the order 150–995 MΩ. The first switching occurs at 1.44 V and at 2.16 V thereafter with a compliance current of 0.5 mA and 1 mA. For the reset process, a 4.8–18.1-mA current flows through the memory cell at voltages of 0.4–0.66 V.

From the I–V characteristics in Fig. 12, when Au is replaced with Pt, it is seen the set operation occurs at voltages between 0.8 V and 2.3 V and the compliance current is limited to 0.5 mA and 1.0 mA. In the reset operation, the memory cell draws a current of 4.9–9.7 mA over the voltage range 0.26–0.52 V. The resistance in the HRS is between of 7 MΩ and 100 MΩ whereas in the LRS, the values are between 79 Ω and 47 Ω, indicating an R_{off}-to-R_{on} ratio of the order of 10^9. Significantly, the device in this case only exhibits unipolar switching.

For the same device when the ZnTe layer was deposited at a distance of 15 cm, the set operation occurs at voltages between 0.72 V and 1.36 V and the compliance current is limited to 0.5 mA and 1 mA. In the reset operation, the memory cell draws a current of 2.1–17 mA for voltages between 0.2 V and 0.74 V. The memory cell resistance, in the HRS, is between 3.2 MΩ and 100 MΩ, whereas in the LRS, the resistance is between 69 Ω and 91 Ω.

It would appear that the electroforming process in all the devices is based on soft breakdown only,

since the current is limited to 0.1–0.6 mA. During the set process also, the current is limited to 0.5–1 mA.

In terms of increasing work function, the bottom electrodes can be placed in the order Al < Au < Pt. In terms of switching, it would appear that the best switching characteristics were observed when Al was the bottom electrode and the band gap of ZnTe was close to that for the stoichiometric compound. Furthermore, this device structure showed the highest value of the HRS, i.e., 5 GΩ, in comparison to values of 33.4 MΩ and 206 MΩ for the devices with Au and Pt as the bottom electrode, respectively. The observed behaviour is also consistent with Eq. 1 which shows that the lower-work-function metal along with the lowest band gap leads to the highest R_{off}-to-R_{on} ratio. The switching characteristics also indicate that band gap engineering can be a very significant tool to manipulate the switching characteristics. It is pertinent to note that band gap variation is a consequence of the change in Zn-to-Te ratio which is a result of variation in rate of evaporation. Thus, a more precise control over rate of evaporation and, hence, the rate of deposition can lead to enhanced switching characteristics. In most cases, the devices failed after 5–7 cycles which is probably due to poor microstructure/morphology and also spatial variations in the Zn-to-Te ratio. Improving endurance and retention is the subject of a concurrent study.

The mechanism of switching in these films is now discussed. To establish the origin of conductivity and its reversibility, double-log I–V plots are plotted as shown in Figs. 13 and 14. These are typical plots that summarize the behaviour. The plots for the device structure Au/ZnTe/Au are displayed in Fig. 13 and those for Au/ZnTe/Ag are presented in Fig. 14. The dielectric constant of the device calculated form the I–V characteristics using Schottky and Poole–Frenkel models and the dielectric constants values at non-ohmic regions of set curves are 0.53 and 6.72, respectively (almost the same for both devices). From the calculated dielectric value, it is evident that in the non-ohmic region of the high-resistance-OFF state (prior to break down) of the device, the conductivity is due to defects (Poole–Frenkel conduction) until the bias reaches a threshold (SET voltage). Beyond this threshold, there is a very large increase in current flow (almost five orders of magnitude in some cases), taking the device into the ON state. The dielectric breakdown causes formation of Zn or Zn-rich conductive paths called filaments resulting in high conductivity. In the ON state, the device is ohmic in nature (Fig. 13a and b), revealing the formation of conductive paths in the ON state. It has been shown earlier by Ota and Takahashi[17] and Burgelman[18] that the conduction in ZnTe layers is a consequence of the formation of conductive filaments. The off-state conductivity is dominated by Poole–Frenkel emission.

The reversibility in conductivity can be explained based on the work on $Cd_{1-x}Zn_xTe$ by Jakubas and Boguslwaski.[23] They observed that reversible conductivity is due to the formation of these Frenkel pairs and the presence of excess free electrons which reduces the energy barrier for the pair generation from 2.5 eV in intrinsic samples to 1.2 eV for doped samples. Experimental evidence suggests that this is the mechanism in the present case, with increase in applied voltage.

CONCLUSIONS

ZnTe thin films have been deposited by thermal evaporation on different substrates. The source–substrate distance was varied between 5 cm and 18 cm. The substrates were not heated during deposition. It is shown that the Zn-to-Te ratio is very sensitive to the source–substrate distance. All the films are crystalline-independent of deposition conditions. The microstructure reveals nanograins at large distances, and sub-micron-sized grains at shorter distances. The films were evaluated for resistive switching behavior using different device structures wherein the bottom electrode is Al, Au or Pt and the top electrode is Al, Au or Ag. It is demonstrated the switching behavior can be engineered using different combinations of metal electrodes and variation of the Zn-to-Te ratio.

ACKNOWLEDGEMENTS

REFERENCES

1. R. Waser and M. Aono, *Nat. Mater.* 6, 833 (2007).
2. A. Sawa, *Mater. Today* 11, 28 (2008).
3. D.S. Jeong, R. Thomas, R.S. Katiyar, J.F. Scott, H. Kohlstedt, A. Petraru, and C.S. Hwang, *Rep. Prog. Phys.* 75, 076502 (2012).
4. D. Ielmini, *Semicond. Sci. Technol.* 31, 063002 (2016).
5. L.D. Varma Sangani, C. Ravi Kumar, and M. Ghanashyam Krishna, *J. Electron. Mater.* 45, 32 (2016).
6. L.D. Varma Sangani, K. Vijaya Sri, M. Ahamad Mohiddon, and M. Ghanashyam Krishna, *RSC Adv.* 5, 67493 (2015).
7. C.B. Lee, B.S. Kang, A. Benayad, M.J. Lee, S.-E. Ahn, and K.H. Kim, *Appl. Phys. Lett.* 9, 04115 (2008).
8. S.R. Lee, H.M. Kim, J.H. Bak, Y.D. Park, K. Char, and H.W. Park, *Jpn. J. Appl. Phys.* 49, 031102 (2010).
9. F. Zhuge, K. Li, B. Fu, H. Zhang, J. Li, H. Chen, L. Liang, J. Gao, H. Cao, Z. Liu, and H. Luo, *AIP Adv.* 5, 057125 (2015).
10. G. Palma, E. Vianello, G. Molas, C. Cagli, F. Longnos, J. Guy, M. Reyboz, C. Carabasse, M. Bernard, and F. Dahmani, *Jpn. J. Appl. Phys.* 52, 04CD02 (2013).
11. D.J. Chadi, *Ann. Rev. Mater. Sci.* 24, 45 (1994).
12. H. Bellakhder, A. Outzourhit, and E.L. Ameziane, *Thin Solid Films* 382, 30 (2001).
13. M.S.R.N. Kiran, S. Kshirsagar, M. Ghanashyam Krishna, and S.P. Tewari, *Eur. Phys. J. Appl. Phys.* 51, 1050 (2010).
14. S. Kshirsagar, M. Ghanashyam Krishna, and S.P. Tewari, *AIP Conf. Proc.* 1349, 1285 (2011).

15. S. Kshirsagar, M. Ghanashyam Krishna, and S.P. Tewari, *Mater. Sci. Semicond. Proces.* 16, 1002 (2012).
16. E. Constable and R.A. Lewis, *J. Appl. Phys.* 112, 063104 (2012).
17. T. Ota and K. Takahashi, *Solid State Electron.* 16, 1089 (1973).
18. M. Burgelman, *Electrocomp. Sci. Technol.* 7, 93 (1980).
19. V. Ananthan and P.B. Phatak, US Patent 20140264241, A1, (2013).
20. K.U.M. Kumar, R. Brahma, M. Ghanashyam Krishna, A.K. Bhatnagar, and G. Dalba, *J. Phys.: Condens. Matter* 19, 496208 (2007).
21. W.D. Baker and A.G. Milnes, *J. Appl. Phys.* 43, 5152 (1972).
22. H.L. Skriver and N.M. Rosengaard, *Phys. Rev. B* 46, 7157 (1992).
23. P. Jakubas and P. Bogusławski, *Phys. Rev. B* 77, 214104 (2008).